Origin of thyrotropin-releasing hormone neurons that innervate the tuberomamillary nuclei

Edith Sánchez-Jaramillo (✉ esanchez@imp.edu.mx)

  Instituto Nacional de Psiquiatría Ramón de la Fuente Muñiz: Instituto Nacional de Psiquiatria Ramon de la Fuente Muniz   https://orcid.org/0000-0002-5560-2645

Gábor Wittmann

  Tufts University New England Medical Center: Tufts Medical Center

Judit Menyhért

  Hungarian Academy of Sciences Institute of Experimental Medicine: Kiserleti Orvostudomanyi Kutatointezet

Praful Singru

  National Institute of Science Education and Research

Gabriela Berenice Gómez González

  UNAM Instituto de Neurobiologia: Universidad Nacional Autonoma de Mexico Instituto de Neurobiologia

Eduardo Sánchez Islas

  Instituto Nacional de Psiquiatría Ramón de la Fuente Muñiz: Instituto Nacional de Psiquiatria Ramon de la Fuente Muniz

Nashiely Yáñez Recendis

  Instituto Nacional de Psiquiatría Ramón de la Fuente Muñiz: Instituto Nacional de Psiquiatria Ramon de la Fuente Muniz

Jaime Arturo Pimentel Cabrera

  Universidad Nacional Autónoma de México Instituto de Biotecnología: Universidad Nacional Autonoma de Mexico Instituto de Biotecnologia

Martha León Olea

  Instituto Nacional de Psiquiatría Ramón de la Fuente Muñiz: Instituto Nacional de Psiquiatria Ramon de la Fuente Muniz

Balazs Gereben

  Hungarian Academy of Sciences Institute of Experimental Medicine: Kiserleti Orvostudomanyi Kutatointezet

Csaba Fekete

  Hungarian Academy of Sciences Institute of Experimental Medicine: Kiserleti Orvostudomanyi Kutatointezet

Jean Louis Charli

  Universidad Nacional Autónoma de México Instituto de Biotecnología: Universidad Nacional Autonoma de Mexico Instituto de Biotecnologia

Ronald Michael Lechan

Tufts University School of Medicine

Research Article

1 **Origin of thyrotropin-releasing hormone neurons that innervate the tuberomamillary nuclei**

2

3 Edith Sánchez-Jaramillo[1]*, Gábor Wittmann[2]*, Judit Menyhért[3], Praful Singru[2, ‡], Gabriela B. Gómez-

4 González[1,4], Eduardo Sánchez-Islas[5], Nashiely Yáñez-Recendis[1], Jaime Arturo Pimentel-Cabrera[6], Martha

5 León-Olea[5], Balázs Gereben[3], Csaba Fekete[2,3], Jean-Louis Charli[4], Ronald M. Lechan[2,7]

6

7

8 [1]Laboratorio de Neuroendocrinología Molecular, Dirección de Investigaciones en Neurociencias, Instituto

9 Nacional de Psiquiatría Ramón de la Fuente Muñiz, CDMX 14370, México.

10 esanchez@imp.edu.mx

11 gabebyre@gmail.com

12 nyare@imp.edu.mx

13 [2]Tupper Research Institute and Department of Medicine, Division of Endocrinology, Diabetes, and Metabolism,

14 Tufts Medical Center, Boston, MA 02111, USA.

15 gabor.wittmann11@gmail.com

16 rlechan@tuftsmedicalcenter.org

17 [3]Department of Endocrine Neurobiology, Institute of Experimental Medicine, Budapest 1083, Hungary.

18 fekete.csaba@koki.mta.hu

19 gereben.balazs@koki.mta.hu

20 [4]Departamento de Genética del Desarrollo y Fisiología Molecular, Instituto de Biotecnología, Universidad

21 Nacional Autónoma de México (UNAM), Cuernavaca, Morelos 62210, México.

22 charli.casalonga@ibt.unam.mx

23 [5]Departamento de Neuromorfología Funcional, Dirección de Investigaciones en Neurociencias, Instituto

24 Nacional de Psiquiatría Ramón de la Fuente Muñiz, CDMX 14370, México.

25 edaxy@imp.edu.mx

26 marthalo@imp.edu.mx

27 [6]Laboratorio Nacional de Microscopia Avanzada, Instituto de Biotecnología, Universidad Nacional Autónoma

28 de México (UNAM), Cuernavaca, Morelos 62210, México.

29   arturo.pimentel@ibt.unam.mx

30   [7]Department of Neuroscience, Tufts University School of Medicine, Boston, MA 02111, USA.

31   rlechan@tuftsmedicalcenter.org

32   ‡ P. Singru present affiliation is School of Biological Sciences, National Institute of Science Education and

33   Research (NISER)-Bhubaneswar, Odisha, 752050, India.

34   pssingru@gmail.com

35

36

37   **Running title:** Origin of TRH neurons that innervate the TMN

38

39

40   *Keywords***:** TRH, histamine, retrograde, anterograde, lateral hypothalamus, *Trh-Cre* transgene

41

42

43   * ESJ and GW contributed equally to this work

44

45   **Corresponding author:** ESJ

Abstract

Hypophysiotropic TRH neurons function as metabolic sensors that regulate the thyroid axis and energy homeostasis. Less is known about the role of other hypothalamic TRH neurons. As central administration of TRH decreases food intake and increases histamine in the tuberomammillary nuclei (TMN), and TMN histamine neurons are densely innervated by TRH fibers from an unknown origin, we mapped the location of TRH neurons that project to the TMN. The retrograde tracer, cholera toxin B subunit (CTB), was injected into the TMN E1-E2, E4-E5 subdivisions of adult Sprague Dawley male rats. TMN projecting neurons were observed in the septum, preoptic area, BNST, perifornical area, anterior PVN, peduncular and tuberal lateral hypothalamus (TuLH), suprachiasmatic nucleus and medial amygdala. However, CTB/pro-TRH178-199 double-labeled cells were only found in the TuLH. The specificity of the retrograde tract-tracing result was confirmed by administering the anterograde tracer, *Phaseolus vulgaris* leucoagglutinin (PHAL) into the TuLH. Double labeled PHAL-pro-TRH boutons were identified in all subdivisions of the TMN. TMN neurons double labeled for histidine decarboxylase (*Hdc*)/PHAL, *Hdc*/*Trhr*, and *Hdc*/*Trh*. Further confirmation of a TuLH TRH neuronal projection to the TMN was established in a transgenic mouse that expresses Cre-recombinase in TRH-producing cells following microinjection of a Cre-recombinase–dependent AAV that expresses mCherry into the TuLH. We conclude that in rodents, the TRH innervation of TMN originates in part from TRH neurons in the TuLH and that this TRH population may contribute to regulate energy homeostasis through histamine *Trhr*-positive neurons of the TMN.

Introduction

Food intake, satiety and energy partition involve activity of hypothalamic neurons that integrate signals from the central and peripheral nervous systems and circulation. The humoral signals include nutrients such as glucose and hormones as leptin, insulin and ghrelin that control the activity of first order sensory neurons in circumventricular organs, and of higher order neurons in the hypothalamus. Among the well-known neuroendocrine output of the brain are the hypophysiotropic neurons in the medial parvocellular region of the PVN that produce thyrotropin-releasing hormone (TRH) and are involved in regulation of the thyroid axis, basal

74 metabolism and thermogenesis (Ishikawa et al. 1988; Kawano et al. 1991; Fekete and Lechan 2014). Additional

75 to its neurohormonal role in thyroid hormone homeostasis, however, TRH has other actions that impact energy

76 balance. For example, the peripheral administration of TRH produces anorexia, an effect that is likely central

77 since TRH administration into the cerebrospinal fluid or directly into the hypothalamus has a rapid, potent

78 anorexigenic effect that is independent of thyroid function (Suzuki et al. 1982; Horita 1998).

79 Histamine neurons contribute to the anorexigenic output from the hypothalamus (Ookuma et al. 1989; Masaki

80 and Yoshimatsu 2007; Panula and Nuutinen 2013). It has been proposed that histamine may mediate the

81 anorexigenic effect of centrally administered TRH, as the effect can be attenuated by pretreatment with an

82 irreversible inhibitor of L-histamine decarboxylase, the rate limiting enzyme for histamine synthesis (Gotoh et

83 al. 2007). In keeping with this observation is that histamine neurons, which are located exclusively in the

84 hypothalamic tuberomamillary nuclei (TMN), are densely innervated by asymmetric TRH boutons (Sarvari et

85 al. 2012), respond to TRH receptor agonists and are activated by TRH *in vitro* (Parmentier et al. 2009). To

86 elucidate the origin of TRH neurons that innervate the TMN, we used a combination of retrograde and

87 anterograde tracers and genetic and viral tools, identifying the tuberal lateral hypothalamic (TuLH) TRH

88 neurons as an origin of the TRH input to the TMN.

89

90 **Materials and Methods**

91 **Animals**

92 Adult male Sprague Dawley rats (Taconic Farms, German Town, NY), eight weeks old weighing 260 – 300 g

93 from Tufts University and adult male and female C57BL/6NJ *Trh-Cre* mice from Instituto de Biotecnología-

94 UNAM colony, eight weeks old weighing 26 – 30 g were used in this study. Animals were acclimatized to

95 standard environmental conditions (rats: lights on between 0600 and 1800 hours, temperature 22°C ± 1°C, rat

96 chow -2918 Envigo- and water *ad libitum*; mice: lights on between 0700 and 1900 hours, temperature 22°C ±

97 1°C, water, and food -Harlan 2018SX- *ad libitum*). Protocols followed the NIH guide for the care and use of

98 laboratory animals (8th ed.), and the Official Mexican Norm for production, care and use of laboratory animals

99 NOM-062-ZOO-1999. All experimental protocols were reviewed and approved by the Institutional Animal

100 Care and Use Committee at Tufts Medical Center and Tufts University School of Medicine and the institutional

4

101   bioethics committee at Instituto de Biotecnología-UNAM and Instituto Nacional de Psiquiatría Ramón de la

102   Fuente Muñiz.

103

104   **Retrograde tract-tracing experiments in rats**

105   The retrograde tracer, cholera toxin ß subunit (CTB; List Biological Laboratories, Campbell, CA), was injected

106   iontophoretically into the hypothalamic tuberomammillary nuclei (TMN), targeting E1-E2 subdivisions at

107   stereotaxic coordinates from the bregma: AP= -3.84 mm, DV= -9.6 mm, L= -1.5 mm (n= 19 rats), or E4-E5

108   subdivisions at AP= -3.84 mm, DV= -9.33 mm, L= 0.33 mm (n= 6 rats; Paxinos 2009). Animals were

109   anesthetized i.p. with ketamine 50 mg/kg, xylazine 10 mg/kg body weight, and their heads mounted in a

110   stereotaxic apparatus with bregma and lambda in the horizontal plane. A glass micropipette with 20 μm outer

111   tip diameter filled with 0.5% CTB in distilled water was lowered into the brain through a burr hole. CTB was

112   iontophoresed by a 6-μA positive current, pulsed on-off at 7-second intervals over 15 minutes, using a constant-

113   current source (Stoelting, Wood Dale, IL). Post-operative analgesia was provided by administering

114   buprenorphine, 0.05 mg/ kg subcutaneously. After a 10 days transport time, animals were deeply anesthetized

115   with ketamine-xylazine and perfused transcardially with 20 ml phosphate buffered saline (PBS; pH 7.4)-

116   heparin, followed by 150 ml of 4% paraformaldehyde- 0.1 M phosphate buffer (PB) at pH 7.4. The brains were

117   removed, immersed in 30% sucrose for 1–2 days, and frozen on dry ice. Serial 25 μm thick coronal sections

118   were cut on a cryostat (Leica CM3050S, Nussloch GmbH, Germany) into one-in-six series of sections and

119   collected into antifreeze solution (30% ethylene glycol; 25% glycerol; 0.05 M PB) to be stored at –20°C until

120   processed for immunohistochemistry. The positions of the injection sites were assessed by immunofluorescent

121   staining. One series of sections were treated with 0.5% H_2O_2 and 0.5% Triton X-100 in PBS for 20 minutes,

122   rinsed 3 times in 0.01 M PBS and incubated for 20 minutes in antibody diluent (2% normal horse serum, 0.2 %

123   Photoflo, 0.2 % sodium-azide in PBS). CTB injection sites were identified by overnight incubation of the

124   sections in goat anti-CTB serum (#703, List Biological Laboratories) at 1:2,000 dilution, and subsequently in

125   Cy3-conjugated donkey anti-goat IgG for 2 h (Jackson Immunoresearch, 1:200 dilution). Sections from brains

126   with accurate injections into the TMN were further incubated overnight in a rabbit antibody against pro-TRH[178-

127   199] (gift from Eva Redei), diluted at 1:50,000. After washes in PBS, the sections were immersed in Alexa 488

128   conjugated donkey anti-rabbit IgG (Jackson Immunoresearch, 1:200 dilution) for 2 h. Sections were rinsed in

129   PBS and once in Tris 0.05 M, pH 7.6, mounted onto glass slides and coverslipped with Vectashield antifade

130   mounting medium with DAPI (Vector Laboratories) for imaging.

131

132   **Immunofluorescence imaging and data analysis (CTB experiments)**

133   Immunofluorescence sections were observed using a Zeiss Axioplan 2 fluorescence microscope. The images

134   were captured using a Spot digital camera (Diagnostic Instrument, Sterling Heights, MI), double exposed while

135   switching filter sets for each fluorochrome, and superimposed in Adobe Photoshop CS4 using a Macintosh G4

136   computer to create a composite image of the same field. Filter sets included an Alexa 488 excitation filter of

137   450 – 490 nm, beam splitter of 495 nm, and emission filter of 500 –550 nm; and Cy3 excitation filter of 538 –

138   562 nm, beam splitter of 570 nm, and emission filter of 570 – 640 nm.

139   Immunofluorescence sections with accurate injections into the TMN were further observed with a Zeiss 510

140   META laser confocal microscope (Carl Zeiss, Germany), using an Argon laser at 488 nm to visualize Alexa

141   488, and a Helium-Neon laser at 543 nm to visualize Cy3. The confocal microscope was attached to an Axiovert

142   200 M microscope with a 63X Plan Apo 1.4 oil objective (Carl Zeiss) for imaging. Prior to the analysis, a

143   lambda stack was made to obtain the emission spectrum for each fluorophore, and barrier filters were placed to

144   separate the fluorescence emission peak and avoid cross-linking of the emission spectrum curves [Alexa

145   488: excitation filter of 450 – 490 nm, beam splitter of 495 nm, and emission filter of 500 –550 nm; Cy3,

146   excitation of 538 –562 nm, beam splitter of 570 nm, and emission filter of 570 – 640 nm]. Confocal images

147   were taken using the "multi-tracking" mode. The image acquisition parameters such as the diameter of the

148   pinhole, the gain detector and the laser power were adjusted to give the adjusted dynamic range in all observed

149   preparations. A Z-stack was obtained from each section with optical cuts of 1 μm size in the Z axis. From the

150   Z-stack, the image with the best immunoreactivity for TRH and CTB colocalization was chosen, and the

151   Manders overlap coefficient analysis was determined with LSM 510, Carl Zeiss 4.0sp1 software. The value of

152   one was considered as total colocalization as referenced by Manders et al. 1993.

153

154   **Anterograde tract-tracing experiments in rats**

155   The anterograde tracer, *Phaseolus vulgaris* leuco-agglutinin (PHAL; Vector Laboratories, Burlingame, CA),

156   was injected iontophoretically into the TuLH of 12 rats as follows. Rats were anesthetized i.p. with ketamine

157   50 mg/kg, xylazine 10 mg/kg body weight, and their heads positioned in a stereotaxic apparatus with bregma

158   and lambda in the horizontal plane. A glass micropipette (20 µm outer tip diameter) filled with 2.5% PHAL in

159   0.01 M PB (pH 8.0) was lowered into the brain through a burr hole in the skull at the following stereotaxic

160   coordinates from the bregma: AP= -2.92 mm, DV= -9.4 mm, L= -1.6 mm corresponding to the TuLH (Paxinos

161   2009). The tracer was deposited by iontophoresis as described above. Rats were allowed to survive for 8 days

162   and then deeply anesthetized with ketamine- xylazine and perfused transcardially with 20 ml 0.01 M PBS (pH

163   7.4), followed by 150 ml of 4% paraformaldehyde in 0.1 M PB, pH 7.4. The brains were rapidly removed, cut

164   into two blocks, and cryoprotected by immersion in 30% sucrose-PBS overnight. The brains were sectioned at

165   25 µm and then collected into antifreeze solution to store at $-20°C$ until used for immunohistochemistry.

166   Sections were pre-treated with 0.5% H_2O_2 and 0.5% Triton X-100 in PBS for 20 minutes. Nonspecific antibody

167   binding was reduced by treatment in 2% normal horse serum in PBS for 20 minutes after which they were

168   incubated overnight in 1:5,000 goat anti-PHAL antiserum (Vector labs) diluted in antibody diluent. After

169   washing in PBS, the sections were incubated in 1:200 Cy3-conjugated donkey anti-goat IgG (Jackson

170   Immunoresearch) for 2 h and rinsed in PBS. Sections from animals with injection sites in the TuLH area were

171   further incubated in rabbit anti-pro-TRH$_{178-199}$ antiserum (1:50,000, overnight), and subsequently in 1:400

172   Alexa 488-conjugated donkey anti-rabbit IgG (Jackson) for 2 h, at RT. Sections were rinsed and mounted as

173   mentioned above. Antibody characterization has been described in detail (Wittmann et al. 2009).

174

175   **Anterograde tract-tracing experiments in mice**

176   The anterograde tracer, PHAL was injected iontophoretically into the TuLH of ten C57BL/6J adult male mice

177   as described for rats, except that the stereotaxic coordinates were from the bregma AP= -1.94 mm, DV= -5.5

178   mm, L= -0.8 mm (Paxinos and Franklin 2001). The tracer was deposited by iontophoresis and mice were

179   allowed to survive for 8 days and then deeply anesthetized with ketamine- xylazine, perfused transcardially

180   with 5 ml 0.01 M PBS (pH 7.4), followed by 50 ml of 3% paraformaldehyde in 0.1 M PB, pH 7.4 / 1% acrolein.

181   The brains were rapidly removed, cryoprotected by immersion in 30% sucrose-PBS overnight, sectioned at 20

182   µm and then either processed for PHAL/HDC floating immunohistochemistry or thaw-mounted on Fisherbrand

183   Superfrost Plus Microscope Slides, air-dried and stored at $-80°C$ until used for double labeling immuno-ISH

184   fluorescence.

185 For immuno-ISH fluorescence, a set of mounted sections from animals with injection sites in the TuLH area

186 (n=3), were hybridized with a histidine decarboxylase (*Hdc*; a gift from Dr. Erik Hrabovszky) fluorescein 12-

187 UTP riboprobe, thoroughly washed, dehydrated and pre-treated with 0.5% H_2O_2 and 0.5% Triton X-100 in PBS

188 to follow the immunodetection protocol. Double immunofluorescence was detected after incubating overnight

189 in 1:5,000 goat anti-PHAL antiserum and 1:100 anti-mouse fluorescein (11426320001, Roche) and

190 subsequently in 1:200 Cy3-conjugated donkey anti-goat IgG and 1:200 Alexa 488 -conjugated donkey anti-

191 mouse IgG for 2 h.

192 For immunohistochemistry, a separated set of floating sections was incubated overnight in 1:5,000 goat anti-

193 PHAL antiserum and 1:5,000 rabbit anti-histidine decarboxylase antiserum (16045, Progen; Yu et al. 2019) and

194 subsequently in 1:400 Alexa 488-conjugated donkey anti-rabbit IgG (Jackson) and 1:200 Cy3-conjugated

195 donkey anti-goat IgG for 2 h, at RT. Sections were rinsed, mounted and processed for immunofluorescence

196 imaging and data analysis as follows.

197

198 **Immunofluorescence imaging and data analysis (PHAL experiments)**

199 For a quick overview, immunofluorescence was observed using a Zeiss Axioplan 2 fluorescence microscope.

200 The images were captured, double exposed while switching filter sets for each fluorochrome, and superimposed

201 in Adobe Photoshop CS4 to create a composite image of the same field as described.

202 Identification of double labelled PHAL/TRH-immunofluorescence profiles in the TuLH or double labelled

203 PHAL/TRH or PHAL/HDC-immunofluorescence fibers in the TMN was determined using a CSU-W1

204 Yokogawa SDC on an inverted Zeiss microscope Observer Z1, equipped with Plan Neo 20X/0.8 NA and Plan

205 Apo 63X/1.4 N.A. Fluorescence was excited with the 488 nm (50 mW) and 561 nm (20 mW) lines diode lasers

206 and collected with a Bright Line FF01-525/30 nm and 617/73 nm respectively. Images were acquired with an

207 Andor iXon 5078 controlled with Slide Book 6.17 software. Multiple stage positions were collected using a

208 WK-XYBH-APZ30-AV00FT ASI stage controller and optical sections were collected using a Z-stage ASI

209 Piezo MS- 2000 Controller.

210 To quantify the degree of colocalization, original images were processed using an ImageJ macro (Schindelin et

211 al. 2012) designed to perform the following procedure. Application of Otsu thresholding (Otsu 1979) over the

212 488 and 561 channels to eliminate background pixels. Then, for each single optical section, a set of filtered

213   pixels 488 (Gi) and 561 (Ri) was used to calculate a specific value for the Object Pearson's coefficient

214   (https://svi.nl/ColocalizationTheory). To illustrate the same set of filtered pixels on each single focal plane, we

215   generated a Pearson colocalization map Mp 3 (https://svi.nl/ColocalizationTheory). A Z-stack obtained from

216   each 488 or 561 thresholded image, with optical cuts of 1 μm size in the Z axis was merged and represented as

217   a composed image using the green and red channels on the ImageJ software (version 2.1.0/1.53h, NIH, USA).

218

219   **Dual-label fluorescence in situ hybridization**

220   Ten μm (mice) or 18 μm (mice and rat) coronal sections were cut from the rostral extent of the hypothalamic

221   lateral hypothalamus to the tuberal lateral hypothalamus (Paxinos 2009; Paxinos and Franklin 2001) using a

222   Leica CM3050 S cryostat, thaw-mounted on Fisherbrand Superfrost Plus Microscope Slides (Thermo Fisher

223   Scientific; Cat #12-550-15), air-dried and stored at –80°C. The mounted sections were fixed with 4%

224   paraformaldehyde - 0.1 M PB (pH 7.4) for 20 min, rinsed in PBS for 5 min, acetylated with 0.25% acetic

225   anhydride in 0.1 M triethanolamine for 10 min, treated with ascending ethanol series (2 min) and chloroform

226   (10 min), partially rehydrated in 95% ethanol, and then processed for in situ hybridization as described (Lazcano

227   et al. 2015; Aguilar-Valles et al. 2007). Two adjacent series of 18 μm thick rat coronal sections, each containing

228   every 12th section, were hybridized with the mixture of the digoxigenin-labeled *Trhr* or digoxigenin-labeled

229   *Trhr2* and either fluorescein-labeled *Trh* or *Hdc* riboprobes. Ten or 18 μm thick mice coronal sections covering

230   the rostro- caudal extent of the TuLH or the TMN were hybridized with a mouse digoxigenin-labeled *Trh* and

231   a fluorescein-labeled *Cre* recombinase riboprobe or a dig- labeled *Trh* and a fluorescein-labeled *Hdc* riboprobe.

232   Sections were incubated overnight at 56°C in a humidified chamber as described (Jones et al. 2019). The *Trhr*,

233   *Trhr2* and *Trh* probes were detected with peroxidase-conjugated, anti-digoxigenin antibody (diluted 1:100 in

234   1% blocking reagent, Roche) and the signal was amplified with the TSA Plus DIG Kit (Cat# NEL748E001KT,

235   Perkin Elmer) for 30 min, using the DIG amplification reagent at 1:500 dilution in 0.05M Tris (pH 7.6)

236   containing 0.01% H_2O_2.

237   Sections were then incubated in a rabbit monoclonal anti-digoxigenin antibody (Thermo Fisher, Cat# 700772;

238   at 1 μg/ml concentration) for 3h in the presence of 2% sodium azide to inactivate peroxidase activity. Sections

239   were thoroughly washed in PBS and incubated overnight in peroxidase-conjugated sheep anti-fluorescein

240   antibody (Roche, Cat# 11426346910; diluted 1:100 in 1% blocking reagent). Signal amplification was applied

9

241 for 30 min using the TSA Plus Biotin Kit (Perkin Elmer) with the TSA Plus biotin reagent diluted 1:300 in

242 0.05M Tris and 0.01% H_2O_2. The biotin deposits and the anti-digoxigenin-antibody were detected with Alexa

243 Fluor 488-conjugated Streptavidin and Alexa 594-conjugated anti-rabbit IgG (Jackson Immunoresearch;

244 1:200), respectively. Sections were rinsed thoroughly in PBS, once in Tris 0.05 M (pH 7.6) and coverslipped

245 with Vectashield antifade mounting medium with DAPI (Vector Laboratories). Immunofluorescence imaging

246 and data analysis were made as described for CTB except that immunofluorescence was observed using a Leica

247 DM 1000 LED fluorescence microscope with a HI PLAN 10X/0.25 or 40X/0.65 objective, and bandpass (BP)

248 filter sets of 340-380/ dichromatic mirror (DM) 400/ barrier LP 425; BP 480/40/DM 505/barrier BP 527/30;

249 BP 560/40/DM595/barrier BP 645/75 for DAPI, Alexa 488 and Alexa 594, respectively.

250 Images were captured using a digital Firewire camera (DFC450C, Leica) and a Leica Application Suite

251 software. Sections were double exposed while switching filter sets for each fluorochrome and superimposed in

252 Adobe Photoshop CS6 using an iMac computer to create a composite image of the same field.

253

254 **Generation of a transgenic mouse line expressing Cre recombinase in TRH-producing cells**

255 A BAC clone (Clone ID: RP23-295F1, http://bacpac.chori.org), containing Mus musculus Trh genomic

256 sequence along with 118.9 kb of 5' flanking sequence and 80.5 kb of 3' flanking sequence of the TRH gene

257 was used to generate TRH-Cre mice. The Cre recombinase coding sequence was inserted +65 bp from the

258 translational start site of TRH gene exon 2, along with a polyadenylation cassette and a kanamycin resistance

259 gene flanked by FRT sites (FKF cassette), to allow selection of recombinants containing the insert. A 3.4 kb

260 long PCR product containing the mTrh flanked by the Cre-polyadenylation cassette-kanamycin amplicon was

261 used to remove the template plasmid. Homologous recombination with electrocompetent cells was induced to

262 insert the 3.4 kb PCR product into the BAC RP23-295F1. The FKF cassette was removed and obtention of a

263 Trh-Cre BAC clone confirmed by sequence.

264 Positive clones were grown on chloramphenicol/ ampicillin resistant plates, scaled into LB antibiotic-resistant

265 media and purified using a commercially available kit (Nucleobond Bac Maxi Kit, BD Biosciences Clontech).

266 The Trh-Cre BAC DNA was used to obtain transgenic founders by pronuclear microinjection of 0.5- 1 ng of

267 circular plasmid into C57BL/6J oocytes using standard procedures by the Tufts Medical Center Transgenic

268 Core Facility. Genotyping of transgenic mice was performed by standard PCR on genomic DNA isolated from

269   tail snips at weaning using primers against pro-TRH exon 1 (mTRH sense primer: 5' -

270   TAGGCACCTTGGCACCCTGAT - 3') and Cre recombinase protein (Cre antisense primer: 5' -

271   CCTGGTCGAAATCAGTGCGTT - 3'). PCR conditions for this reaction were: 94°C for 2 min, [94°C for 45s,

272   60°C for 30s, 72°C for 1:30 min] x 30 cycles, 72°C for 10 min, store at 4°C. These primers generate a 600 bp

273   band only in transgenic mice. The IL-2 gene was amplified as an internal control; IL-2 sense: 5′ -

274   CTAGGCCACAGAATTGAAATATCT- 3′, IL-2 antisense: 5′-GTAGGTGGAAATTCTAGCATCATCC -

275   3′. PCR conditions used for this reaction were [94°C for 30s, 60°C for 1 min, 72°C for 30s] x 29 cycles, 72°C

276   for 2 min, store at 4°C. These primers generate a 350 bp band in all animals. Germline transmission was verified

277   by cross-breeding TRH-Cre positive founders with wild-type C57BL/6J mice. To maintain the TRH-Cre

278   transgenic line, all subsequent crosses were performed using pure C57BL/6J mice in Boston, MA USA or pure

279   C57BL/6JN in Cuernavaca, Morelos, México.

280

281   **Mapping of TuLH *Trh* neurons in *Trh-Cre* transgenic mice transduced with a Cre-recombinase–**

282   **dependent adeno-associated virus (AAV)**

283   *Trh-Cre* mice generated in our laboratories (see above) were bilaterally injected by stereotaxic administration

284   of an AAV carrying a *Cre*-dependent hM3D(Gq)-mCherry transgene (AAV-hSyn-DIO-hM3D(Gq)-mCherry,

285   UNC Vector Core Services, Chapel Hill, NC) at a rate of 100 nl /min $(1x10^9$ Pfu) with a 20 µm external diameter

286   glass capillary and a World Precision injector (Nanoliter 2010 # 4878); Bregma: AP= -1.94 mm, DV= -5.4 mm,

287   L= 0.9 mm (n= 10 female; n= 5 male) (Paxinos and Franklin 2001). The scalp was sutured, the animal placed

288   on a heating pad until full recovery from surgery and then returned to its home cage; buprenorphine

289   (0.03 mg/ kg body weight; s.c.) was administered once a day for 2 days after injection. Six weeks later, to allow

290   the expression of hM3Dq-mCherry in the TuLH, animals were deeply anesthetized with ketamine (100 mg/Kg)

291   and xylazine (10 mg/Kg), perfused transcardially with 10 ml PBS, pH 7.4, followed by 50 ml of 4%

292   paraformaldehyde in 0.1 M PB, pH 7.4 and their brains dissected and cryoprotected by immersion in 30%

293   sucrose-PBS overnight. The brains were sectioned at 20 µm and then collected to verify the position of the

294   injection and the status of TRH neurons by standard double immunohistochemistry as described above. Sections

295   were incubated in mouse pro-TRH$_{178-200}$ antiserum (1:1000) raised in rat (Péterfi et al 2018) and rabbit red

296   fluorescent protein (RFP) antiserum (1:1000, Cat. # 600-401-379, Rockland) overnight at RT. After washing,

297   sections were incubated in 1:200 Alexa 488-conjugated donkey anti-rat IgG (Jackson Immunoresearch) and

298   1:200 Alexa 594-conjugated donkey anti-rabbit IgG (Jackson Immunoresearch) for 2 h. Sections were rinsed

299   and mounted as described above. Immunofluorescence was observed using a Leica DM 1000 LED fluorescence

300   microscope as described above. For a general view and a selection of the regions of interest, images were

301   captured using a digital Firewire camera (DFC450C, Leica) and a Leica Application Suite software. Sections

302   were double exposed while switching filter sets for each fluorochrome and superimposed in Adobe Photoshop

303   CS6 using an iMac computer to create a composite image of the same field.

304   Confirmation of double labelled mCherry/ TRH-immunofluorescence in the TuLH or double labelling of

305   mCherry/TRH-immunofluorescence fibers in the TMN was determined using a CSU-W1 Yokogawa SDC on

306   an inverted Zeiss microscope Observer Z1 as described above. Fluorescence was excited with the 488 nm (50

307   mW) and 561 nm (20 mW) lines diode lasers and collected with a BrightLine FF01-525/30 nm and 617/73 nm

308   respectively. Images were acquired with an Andor iXon 5078 controlled with Slide Book 6.17 software.

309   Multiple stage positions were collected using a WK-XYBH-APZ30-AV00FT ASI stage controller and optical

310   sections were collected using a Z-stage ASI Piezo MS- 2000 Controller. The analysis of colocalization was

311   made as described for PHAL. A Z-stack obtained from each 488 or 561 thresholded images, with optical cuts

312   of 1 μm size in the Z axis was merged and represented as a composed image, pseudo-coloring the green and red

313   images from the ImageJ software (version 2.1.0/1.53h, NIH, USA) with Adobe Photoshop CS6 to highlight

314   colocalization.

315

316   **Results**

317   **Distribution of cell bodies retrogradely-labeled with CTB injected into the rat TMN**

318   The origin of cell bodies projecting to the TMN was identified with the retrograde tracer, CTB. The core

319   injection site covered the dorsal TMN (dTMN, E4-E5 regions) in four of six animals, while the core for the

320   ventral TMN (vTMN, E1-E2 regions) was well positioned in ten of nineteen animals. vTMN cores were

321   confined to the border of E1-E2 in 3 animals, diffused slightly from E1-E2 in other 3 animals and was confined

322   to E1 in 4 animals. Representative CTB injection cores are shown in Figure 1. After 10 days of transport, CTB

323   neurons were found primarily ipsilateral to the injection sites, with fewer labeled neurons on the contralateral

324   side. CTB afferents to the dTMN and vTMN were visualized in the septum, medial, central and lateral preoptic

325   area, bed nucleus of the stria terminalis, anterior parvocellular PVN, anterior hypothalamus, peduncular part of

326   the lateral hypothalamus (LH), perifornical lateral hypothalamus (PeFLH), tuberal lateral hypothalamus

327   (TuLH), suprachiasmatic nucleus and medial amygdala.

328   To identify the origin of TRH neurons that innervate the TMN, we conducted dual-label immunofluorescence

329   detection of CTB and pro-TRH$_{178-199}$. Except for the TuLH, none of the nuclei listed above showed

330   colocalization (Figure 2). The retrogradely-labeled TRH neurons from the TuLH were counted in 6 of 14 brains

331   with a successful CTB injection (60 ± 12 TRH cells). Colocalization of CTB/ pro-TRH immunoreactivity was

332   identified in 64 % of TRH cells in 2 rats in which injections were made into the dorsal TMN (E4-E5 regions),

333   68% of TRH cells in 2 rats in which injections were made into the ventral E1 TMN and 92 % of TRH cells in

334   2 rats in which injections were made into the ventral E2 TMN. However, the number of TuLH TRH cells

335   targeted with a vTMN E2 injection, was statistically different from vTMN E1 or dTMN E4-E5 injection (P =

336   <0.001; One-Way ANOVA and multiple comparison test Kruskal-Wallis on Ranks).

337

338   **Immunolocalization of PHAL/pro-TRH-immunoreactive (IR) axon terminals in the rat TMN**

339   Anterograde PHAL labeling in the TuLH confirmed the specificity of the CTB tract-tracing result. PHAL

340   immunolabeling demonstrated highly discrete injection sites fully covering the TuLH rostro-caudally in five of

341   twelve animals and filling dozens of clearly labeled perikarya per section (Figure 3A-C). Acquisition of the

342   same sample in different focal planes allowed us to identify TRH+/PHAL+ positive cells, apparently negative

343   for one or the other immunolabeling in one focal plan, in the core (Figure 3A vs 3B). PHAL-IR fibers were

344   visualized throughout the hypothalamus, reaching the medial and lateral preoptic area, horizontal limb of

345   diagonal band, periventricular hypothalamic nuclei, ventrolateral hypothalamic nuclei, anterior hypothalamus,

346   perifornical and peduncular part of the lateral hypothalamus, medial bed nucleus of the stria terminalis,

347   accessory neurosecretory nucleus; anterior, medial and posterior parvicellular PVN; anterior and lateromedial

348   magnocellular PVN, medial forebrain bundle, paraterete and terete of the hypothalamus, anterior hypothalamus

349   in its posterior part, dorsal and medial arcuate, latero-posterior arcuate; dorsal, central and ventral dorsomedial

350   hypothalamus; posterior hypothalamus, mammillothalamic tract, ventral premammillary nuclei and dorsal and

351   ventral tuberomammillary nuclei. Double-labeled immunofluorescent PHAL/ pro-TRH$_{188-199}$ containing axon

352   terminals or en-passant boutons were identified in the dorsal (E4-E5) and ventral (E1-E2) regions of the TMN,

13

353 with a density of PHAL/pro-TRH immunoreactive fibers low for E4, medium for E5 and high for E2 (Figure

354 3D-F).

355

356 **Fluorescent in situ hybridization in the TuLH and TMN**

357 *Trh* mRNA was mapped in coronal sections containing the TuLH or TMN of adult male rats (n=3). Dorso-

358 ventrally, *Trh* mRNA positive cells in the TuLH were observed below the fornix, between the dorsomedial and

359 the ventromedial hypothalamic nuclei (Figure 4A). *Trh* positive cells were also observed in the TMN itself,

360 including E3, E4-E5 and along E1-E2 (Figure 4B,C). *Hdc* mRNA positive cells showed a distribution pattern

361 similar to that observed for *Trh* mRNA both in the rat (Figure 4B-D) and the mouse (Figure 5A,B) TMN. In

362 mice, the *Trh* population represented 46% ± 5 of the TMN cells stained with DAPI (182 ± 6 cells) while

363 histamine cells 39% ± 2. By double labelling we observed that 75% ± 7 of *Trh* cells express *Hdc* and 82% ± 5

364 of *Hdc* cells express *Trh* (Figure 5A,B).

365 In addition, *Hdc* mRNA, or immunoreactive HDC, positive cells were reached by immunoreactive PHAL

366 positive fibers whose cell bodies were originated in the mouse TuLH (Figure 6A,B). Double labelling for *Hdc*

367 mRNA and *Trhr* or *Trhr2* mRNA in the E4-E5 or E1-E2 subdivisions of rat TMN revealed that 53% of the *Hdc*

368 cells co-labeled with *Trhr* mRNA (30 ± 1 *Hdc+/Trhr+* positive cells per field; n=2 fields/ slice/ hemisphere)

369 and 0.6% co-labeled with *Trhr2* mRNA (0.2 ± 0.1 *Hdc+/Trhr2+* positive cells per field; n=2 fields/ slice/

370 hemisphere). Representative images are shown in Figure 7.

371

372 **TRH TuLH-TMN projection in mice**

373 *Trh-Cre* transgenic mice were developed in our laboratories (see above) and germline transmission verified and

374 maintained by cross-breeding *Trh-Cre* positive mice with pure C57/BL6/N (Tufts) or C57/BL6/NJ (UNAM)

375 mice per +10 generations. The expression of GFP or ß-Gal in *Trh-Cre* positive mice was promoted by crossing

376 the *Trh-Cre* mice with reporter mice Z-EG/GFP, or ROSA 26/Lac Z, flanked by Lox-P sequences (Figure 8A,

377 Supplemental Figures S1, S2). The distribution of cells expressing GFP in the CNS was identical to that of *Trh*

378 cells including the olfactory bulb, ventrolateral and medial preoptic area, periventricular hypothalamus,

379 anterior, medial and posterior parvicellular PVN (Supplemental Figure S1). Figure 8A shows distribution of

380 GFP in the peduncular and perifornical part of the lateral hypothalamus, tuberal lateral hypothalamus, dorsal

381 and ventral dorsomedial hypothalamus, medial tuberal nuclei and arcuate nucleus. Sections from the progeny

382 of the *Trh-Cre* mice hybridized with a fluorescent *Trh* or *Cre* mRNA riboprobe showed an identical distribution

383 pattern in the PVN or thalamus (Supplemental Figure S2A). Double labelling FISH for *Trh* and *Cre* mRNA in

384 18 μm thick sections (n=3 male mice) in the TuLH revealed 80±4 *Trh* positive cells or 82±1 *Cre* positive cells

385 corresponding to 18% ± 1 (in each case) of the total number of DAPI nuclei (412±19); furthermore, we detected

386 that 85% ± 2 of *Cre+* cells expressed *Trh*. If FISH was applied to 10 μm thick sections (n=3 male mice), 75±2

387 *Trh* positive cells or 72±5 *Cre* positive cells were counted; 93% ± 5 of *Cre+* cells expressed *Trh* (Figure 8B).

388 Additionally, radioactive ISH for *Trh* mRNA or ß-Gal-IR in the progeny of the *Trh-Cre* x ROSA 26/LacZ

389 indicator mice showed that the distribution pattern for ß-Gal-immunoreactivity was similar to that of *Trh*

390 neurons (Supplemental Figure S2B,C). Finally, double-labeling immunofluorescence for ß-Gal/growth

391 hormone (GH) or ß-Gal/thyroid-stimulating hormone (TSH) in the progeny of *Trh*-Cre x ROSA 26/LacZ mice

392 confirmed previous observations of co-localization for TRH in GH-producing cells (corresponding to less than

393 5% of the GH cell population) and no co-localization in TSH- (Supplemental Figure S2) or adrenocorticotropic

394 hormone-producing cells (not shown).

395

396 **Origin of TRH neurons innervating the TMN in *Trh-Cre* transgenic mice**

397 TRH neuronal projections from the TuLH were mapped in the *Trh-Cre* transgenic mice using a Cre-

398 recombinase–dependent adeno-associated virus (AAV-hSyn-DIO-hM3D(Gq)-mCherry). After six weeks of

399 viral transduction, mCherry cell bodies and dendrites were found in the injected side of the TuLH (Figure 8C).

400 mCherry fibers were also widely distributed in low to medium density in the lateral septum, ventrolateral and

401 medial preoptic area, anterior, medial and posterior parvicellular PVN, dorsal and ventral dorsomedial nucleus,

402 lateral and ventrolateral peduncular part of the hypothalamus and the perifornical part of the lateral

403 hypothalamus surrounding the dorsal and ventral TMN (Figure 8D). Many double-labeled immunofluorescent

404 mCherry and pro-TRH$_{188-199}$ containing cell bodies and fibers were visualized in the TuLH (Figure 9). Axon

405 terminals and/or en-passant boutons originating from the virally infected TRH neurons in the TuLH were

406 present in all subdivisions of the TMN, in both sexes (Figure 9).

407

408

Discussion

Central administration of TRH has a potent anorexigenic effect (Suzuki et al., 1982; Horita 1998), mediated in part through histamine neurons from the TMN (Gotoh et al. 2007). Our data demonstrate that neurons from dorsal and ventral TMN receive inputs from the septum, preoptic area, BNST, PeFx, anterior and medial PVN, VMN, DMN, peduncular LH and TuLH among others, as previously described (Ericson et al. 1991; Haas et al. 2008), but that TRH cells projecting to the TMN are localized in the TuLH. The origin of the TRH input to the TMN was established by mapping the TRH neurons with two complementary tracers in the rat, and anterograde tracing in transgenic *Trh-cre* mice transduced with a Cre-recombinase-dependent AAV. These studies demonstrate that TMN axon terminals or en-passant boutons containing TRH originate at least in part from the TuLH, but we cannot discard that they may also come from TMN neurons that co-express *Trh* and *Hdc*. TRH terminals originating in the TuLH may impinge on histaminergic neurons in all subdivisions of the TMN, where approximately half of the histaminergic neurons co-express *Trhr*.

Histamine neurons are involved in many functions, including alertness, sleep, memory and feeding (Haas and Panula 2003). As these neurons are densely innervated by TRH terminals forming asymmetric synapses (Sarvari et al. 2012), central administration of TRH increases histamine concentration in the TMN (Gotoh et al. 2007) and has a depolarizing effect on histaminergic neurons (Parmentier et al. 2009), we hypothesize that TRH arising from neurons in the TuLH, and possibly from the TMN itself, may mediate some of these responses. TRH neurons of the lateral hypothalamus constitute a large population, distinct from orexin and melanin-concentrating hormone neurons (Horjales-Araujo et al. 2014), but their functional importance is unknown. As TuLH neurons have a predominant glutamatergic phenotype (Ziegler et al. 2002; Stuber and Wise 2016) and the TMN receives excitatory glutamatergic inputs from the lateral hypothalamus (Jang 2014; Yin et al. 2019), co-transmission of TRH/glutamate on some of the histamine neurons may contribute to the excitability of these cells and to physiological arousal. Hypothalamic neuronal histamine regulates the sleep–wake cycle via reciprocal connections to the ventrolateral preoptic area, also known as the ''sleep center'' and therefore, activation of the histamine-TRH-R cells by TuLH-TRH/glutamate, and/or possibly TRH/histamine neurons from the TMN itself, may constitute a neuronal network that regulates arousal.

Unfortunately, our efforts to perform triple labeling to show proTRH-containing PHAL fibers innervating histaminergic neurons have been unsuccessful because commercially available histidine decarboxylase antisera

437 are raised in a species that cross-reacts with the other two immunofluorescent labels. However,

438 immunoreactivity of PHAL on *Hdc* mRNA or HDC-IR positive cells in the TMN (Figure 6A,B) and TMN

439 TRH+/PHAL+ fibers originating from cell bodies in the TuLH (Figure 3), strongly suggest that part of the

440 abundant TRHergic innervation of the histamine neurons comes from the TuLH, and that half of the *Hdc* TMN

441 neurons sense TuLH TRH inputs since they express *Trhr*.

442 The lateral hypothalamus belongs to the reticulate zone of the hypothalamus, containing cell aggregates that

443 lack precise limits. Despite significant progress about the anatomical regionalization and chemical subsets of

444 the LH, differentiation of functional subgroups as mediators of feeding and energy balance responses has

445 remained challenging. Supportive data show that every histologically recognizable subdivision of the LH

446 projects to many nuclei, and although it indicates a lack of specialization, it may be necessary for the integration

447 of behavioral responses. The TuLH, itself, has been divided into at least in 6 sub-regions: tuber cinereum,

448 medial tuberal nucleus, part 1 or part 2 of the medial tuberal nucleus, dorsal tuberal nucleus, lateral tuberal

449 nucleus and magnocellular tuberal nucleus (Geeraedts et al. 1990; Hahn and Swanson 2010). We observed TRH

450 neurons within the lateral and medial TuLH, confirming earlier studies (Airaksinen et al. 1992; Horjales-Araujo

451 et al. 2014). Collectively, the TuLH establishes broad intrahypothalamic connections, particularly to the medial

452 hypothalamus including the periventricular and perifornical zone, the DMN, anterior and intermediate

453 periventricular nuclei and the parvicellular region of the paraventricular nucleus (Saper et al. 1979; this study).

454 Therefore, it has the potential to strongly influence neuroendocrine control mechanisms.

455 Studies by Anand and Brobeck 1951 showed that lesioning the TuLH but not the adjacent "satiety center"

456 VMN, results in complete absence of spontaneous eating, implicating the TuLH as a responsive nucleus for

457 hunger or the urge to eat. Behavioral responses including a lack of interest even for palatable foods or water,

458 persist for several weeks until spontaneous recovery. However, these animals remain leaner than their paired

459 fed controls over their lifespan. While animals with TuLH lesions in the medial zone can recover feeding after

460 injury, ablation of TuLH neurons in the lateral zone produces a more drastic response, as these animals do not

461 survive (Bernardis and Bellinger 1996). Indeed, studies using electrical stimulation of the lateral TuLH have

462 shown it influences a wide variety of autonomic responses including thermoregulatory, ingestive and affective

463 behaviors (Bernardis and Bellinger 1996) that may contribute to the increased mortality in these animals when

464 lesioned.

465 Our ISH data indicate that while TRH neurons from the medial TuLH are in a position to influence

466 hypothalamic nuclei related to energy homeostasis, TRH neurons from the lateral TuLH might exert broader

467 effects. *Trh-Cre* AAV mCherry positive perikarya from the TuLH give rise to fibers ascending into the lateral

468 septum, ventrolateral, medial preoptic area, anterior, medial and posterior PVN as well as the dorsal and ventral

469 DMN in addition to descending fibers in the dorsal and ventral TMN (Figures 8, 9). Furthermore, electrical

470 activity of lateral TuLH neurons gives rise to deep-sleep-wake responses and activity changes related to

471 behavior (Ono et al. 1986). In addition, as the TuLH is traversed by the medial forebrain bundle (Geeraedts et

472 al. 1990), allowing intimate contact with both descending fibers from the basal olfactory, septum, amygdala,

473 nucleus accumbens and, ascending fibers from the brainstem regions, including the VTA, TRH neurons from

474 the TuLH are potentially in a position to participate in the integration of feeding responses as part of the reward

475 and pleasure systems driven by dopamine, GABA and glutamate neurons from the VTA-tuberal LH pathway.

476 Thus, TRH neurons from the TuLH, may function as a relay center in the viscerosensory and visceromotor

477 pathways that impinge on TMN neurons, relaying information onto second order neurons and to the cortex.

478 However, whether the TRH/glutamate TuLH neurons can be activated by hedonic food remains unknown.

479 Furthermore, since TuLH TRH neurons innervate more fully TMN E2 than TMN E4-E5 neurons, and ventral

480 TMN E1-E2 lesions induce hyperphagia but dorsal TMN E4-E5 lesions induce polydipsia, independent of food

481 intake (Mahia and Puerto 2006), investigating the relationship between these functional and anatomical

482 differences is warranted.

483 While most of histamine neurons co-express GABA, various populations of histaminergic TMN neurons also

484 contain neuropeptides (Haas and Panula 2003). Contrary to Airaksinen et al., who showed that only 14% of

485 histamine neurons were positive for TRH-IR in the rat and none in the mice TMN (Airaksinen et al. 1992), we

486 demonstrated that most of the histamine neurons coexpress *Trh* mRNA in mice (Figure 5). Assuming that *Trh*

487 mRNA is indeed translated and pro-TRH processing generates TRH in the histamine neurons, differences may

488 arise from fixative methods used by Airaksinen et al. 1992, who needed colchicine and glutaraldehyde fixation

489 to visualize the mature TRH peptide in the rat TMN. An important question is the role of pro-TRH derived

490 peptides in histamine neurons; are they used locally, and/or do they act together with histamine and GABA in

491 their target regions?. Histamine and pro-TRH derived peptides interact functionally in various target regions.

492 Prepro-TRH$_{178-199}$ modulate histaminergic inputs to the PVN that control neuroendocrine outputs (Fukagawa et

493 al. 2007). TRH and histamine interact in arousal mechanisms in the rat nucleus accumbens (Bristow and Bennett

494 1989). Whether pro-TRH-derived peptides involved in these actions originate in TMN neurons remains

495 unknown.

496 We conclude that TRH neurons from the TuLH have direct projections to the TMN where they could exert

497 effects on histamine/TRH neurons and potentially other neuronal populations. This interaction is likely of

498 excitatory nature and, may involve the co-release of glutamate. The control of histamine neurons by TRH

499 neurons arising from the TuLH may contribute to the well-known effects of histamine on arousal, energy

500 homeostasis, lipid metabolism and/or thermogenesis.

501

502

503 **References**

504 Aguilar-Valles A, Sanchez E, de Gortari P, Garcia-Vazquez AI, Ramirez-Amaya V, Bermudez-Rattoni F,
505   Joseph-Bravo P (2007) The expression of TRH, its receptors and degrading enzyme is differentially
506   modulated in the rat limbic system during training in the Morris water maze. Neurochem Int 50(2):404-
507   417. doi:10.1016/j.neuint.2006.09.009
508 Airaksinen MS, Alanen S, Szaba E, Visser TJ, Panula P (1992) Multiple neurotransmitters in the
509   tuberomammillary nucleus: comparison of rat, mouse, and guinea pig. J Comp Neurol 323(1):103-
510   116. doi:10.1002/cne.903230109
511 Anand BK, Brobeck JR (1951) Localization of a "feeding center" in the hypothalamus of the rat. Proc Soc Exp
512   Biol Med 77(2):323-4. doi: 10.3181/00379727-77-18766.
513 Bernardis LL, Bellinger LL (1996) The lateral hypothalamic area revisited: ingestive behavior. Neurosci
514   Biobehav Rev 20(2):189-287. doi:10.1016/0149-7634(95)00015-1
515 Bristow LJ, Bennett GW (1989) Effect of chronic intra-accumbens administration of the TRH analogue
516   CG3509 on histamine-induced behaviour in the rat. Br J Pharmacol 97(3):745-52. doi: 10.1111/j.1476-
517   5381.1989.tb12012.x
518 Ericson H, Blomqvist A, Kohler C (1991) Origin of neuronal inputs to the region of the tuberomammillary
519   nucleus of the rat brain. J Comp Neurol 311(1):45-64. doi:10.1002/cne.903110105
520 Fekete C, Lechan RM (2014) Central regulation of hypothalamic-pituitary-thyroid axis under physiological and
521   pathophysiological conditions. Endocr Rev 35(2):159-194. doi:10.1210/er.2013-1087
522 Fukagawa T, Fukagawa K, Gotoh K, Noguchi H, Yoshimatsu H (2007) Prepro-TRH 178-199 inhibits
523   histamine- or restraint stress-induced activation of corticotropin releasing hormone production in rat
524   hypothalamus. Obes Res Clin Pract 1(2):I-II. doi: 10.1016/j.orcp.2007.01.002
525 Geeraedts LM, Nieuwenhuys R, Veening JG (1990) Medial forebrain bundle of the rat: IV. Cytoarchitecture of
526   the caudal (lateral hypothalamic) part of the medial forebrain bundle bed nucleus. J Comp Neurol
527   294(4):537-568. doi:10.1002/cne.902940404
528 Gotoh K, Fukagawa K, Fukagawa T, Noguchi H, Kakuma T, Sakata T, Yoshimatsu H (2007) Hypothalamic
529   neuronal histamine mediates the thyrotropin-releasing hormone-induced suppression of food intake. J
530   Neurochem 103(3):1102-1110. doi:10.1111/j.1471-4159.2007.04802.x
531 Haas H, Panula P (2003) The role of histamine and the tuberomamillary nucleus in the nervous system. Nat
532   Rev Neurosci 4(2):121-130. doi:10.1038/nrn1034
533 Haas HL, Sergeeva OA, Selbach O (2008) Histamine in the nervous system. Physiol Rev 88(3):1183-1241.
534   doi:10.1152/physrev.00043.2007
535 Hahn JD, Swanson LW (2010) Distinct patterns of neuronal inputs and outputs of the juxtaparaventricular and
536   suprafornical regions of the lateral hypothalamic area in the male rat. Brain Res Rev 64(1):14-103.
537   doi:10.1016/j.brainresrev.2010.02.002

538 Horita A (1998) An update on the CNS actions of TRH and its analogs. Life Sci 62(17-18):1443-1448.
539   doi:10.1016/s0024-3205(98)00087-3
540 Horjales-Araujo E, Hellysaz A, Broberger C (2014) Lateral hypothalamic thyrotropin-releasing hormone
541   neurons: distribution and relationship to histochemically defined cell populations in the rat.
542   Neuroscience 277:87-102. doi:10.1016/j.neuroscience.2014.06.043
543 Ishikawa K, Taniguchi Y, Inoue K, Kurosumi K, Suzuki M (1988) Immunocytochemical delineation of
544   thyrotrophic area: origin of thyrotropin-releasing hormone in the median eminence.
545   Neuroendocrinology 47(5):384-388. doi:10.1159/000124943
546 Jang IS (2014) Metabotropic glutamate receptors inhibit GABA release in rat histamine neurons. Neurosci Lett
547   579:106-109. doi:10.1016/j.neulet.2014.07.022
548 Jones GL, Wittmann G, Yokosawa EB, Yu H, Mercer AJ, Lechan RM, Low MJ (2019) Selective Restoration
549   of Pomc Expression in Glutamatergic POMC Neurons: Evidence for a Dynamic Hypothalamic
550   Neurotransmitter Network. eNeuro 6(2) e0400-18. doi:10.1523/ENEURO.0400-18.2019
551 Kawano H, Tsuruo Y, Bando H, Daikoku S (1991) Hypophysiotrophic TRH-producing neurons identified by
552   combining immunohistochemistry for pro-TRH and retrograde tracing. J Comp Neurol 307(4):531-
553   538. doi:10.1002/cne.903070402
554 Lazcano I, Cabral A, Uribe RM, Jaimes-Hoy L, Perello M, Joseph-Bravo P, Sánchez-Jaramillo E, Charli JL
555   (2015) Fasting Enhances Pyroglutamyl Peptidase II Activity in Tanycytes of the Mediobasal
556   Hypothalamus of Male Adult Rats. Endocrinology 156(7): 2713-2723. doi:10.1210/en.2014-1885
557 Mahia J, Puerto A (2006) Lesions of tuberomammillary nuclei induce differential polydipsic and hyperphagic
558   effects. Eur J Neurosci 23(5) :1321-1331. doi:10.1111/j.1460-9568.2006.04644.x
559 Manders EMM VF, Aten JA et al (1993) Measurement colocalization of objects in dual-colours confocal
560   images. J Microscopy169:375-382.
561 Masaki T, Yoshimatsu H (2007) Neuronal histamine and its receptors in obesity and diabetes. Curr Diabetes
562   Rev 3(3):212-216. doi:10.2174/157339907781369002
563 Ono T, Sasaki K, Nishino H, Fukuda M, Shibata R (1986) Feeding and diurnal related activity of lateral
564   hypothalamic neurons in freely behaving rats. Brain Res 373(1-2):92-102. doi:10.1016/0006-
565   8993(86)90319-7
566 Ookuma K, Yoshimatsu H, Sakata T, Fujimoto K, Fukagawa F (1989) Hypothalamic sites of neuronal histamine
567   action on food intake by rats. Brain Res 490(2):268-275. doi:10.1016/0006-8993(89)90244-8
568 Otsu NA (1979) Threshold Selection Method from Gray-Level Histograms. In: IEEE Transactions on Systems,
569   Man and Cybernetics 9(1):62-66. doi: 10.1109/TSMC.1979.4310076.
570 Panula P, Nuutinen S (2013) The histaminergic network in the brain: basic organization and role in disease. Nat
571   Rev Neurosci 14(7):472-487. doi:10.1038/nrn3526
572 Parmentier R, Kolbaev S, Klyuch BP, Vandael D, Lin JS, Selbach O et al (2009) Excitation of histaminergic
573   tuberomamillary neurons by thyrotropin-releasing hormone. J Neurosci 29(14):4471-4483.
574   doi:10.1523/JNEUROSCI.2976-08.2009
575 Paxinos G, Watson C (2009) The Rat Brain in Stereotaxic Coordinates, 6th edn. Academic Press, China.
576 Paxinos G, Franklin KBJ (2001) The Mouse Brain in Stereotaxic Coordinates, 2nd edn. Academic Press, San
577   Diego.
578 Péterfi Z, Farkas E, Nagyunyomi-Sényi K, Kádár A, Ottó S, Horváth A, Füzesi T, Lechan RM, Fekete C (2018)
579   Role of TRH/UCN3 neurons of the perifornical area/bed nucleus of stria terminalis region in the
580   regulation of the anorexigenic POMC neurons of the arcuate nucleus in male mice and rats. Brain
581   Struct Funct 223(3):1329-1341. doi: 10.1007/s00429-017-1553-5.
582 Saper CB, Swanson LW, Cowan WM (1979) An autoradiographic study of the efferent connections of the
583   lateral hypothalamic area in the rat. J Comp Neurol 183(4):689-706. doi:10.1002/cne.901830402
584 Sarvari A, Farkas E, Kadar A, Zseli G, Fuzesi T, Lechan RM, Fekete C (2012) Thyrotropin-releasing hormone-
585   containing axons innervate histaminergic neurons in the tuberomammillary nucleus. Brain Res
586   1488:72-80. doi:10.1016/j.brainres.2012.10.010
587 Schindelin J, Arganda-Carreras I, Frise E, Kaynig V, Longair M, Pietzsch T, Preibisch S, Rueden C, Saalfeld
588   S, Schmid B, Tinevez JY, White DJ, Hartenstein V, Eliceiri K, Tomancak P, Cardona A (2012) Fiji:
589   an open-source platform for biological-image analysis. Nat Methods 9(7): 676-682. doi:
590   10.1038/nmeth.2019
591 Stuber GD, Wise RA (2016) Lateral hypothalamic circuits for feeding and reward. Nat Neurosci 19(2):198-
592   205. doi:10.1038/nn.4220

593 Suzuki T, Kohno H, Sakurada T, Tadano T, Kisara K (1982) Intracranial injection of thyrotropin releasing
594 hormone (TRH) suppresses starvation-induced feeding and drinking in rats. Pharmacol Biochem
595 Behav 17(2):249-253. doi:10.1016/0091-3057(82)90078-8
596 Wittmann G, Fuzesi T, Singru PS, Liposits Z, Lechan RM, Fekete C (2009) Efferent projections of thyrotropin-
597 releasing hormone-synthesizing neurons residing in the anterior parvocellular subdivision of the
598 hypothalamic paraventricular nucleus. J Comp Neurol 515(3):313-330. doi:10.1002/cne.22017
599 Yin D, Dong H, Wang TX, Hu ZZ, Cheng NN, Qu WM, Huang ZL (2019) Glutamate Activates the
600 Histaminergic Tuberomammillary Nucleus and Increases Wakefulness in Rats. Neuroscience 413:86-
601 98. doi:10.1016/j.neuroscience.2019.05.032
602 Ziegler DR, Cullinan WE, Herman JP (2002) Distribution of vesicular glutamate transporter mRNA in rat
603 hypothalamus. J Comp Neurol 448(3):217-229. doi:10.1002/cne.10257
604
605
606 **Statements & Declarations**
607
608 **Acknowledgments**

614

615 **Funding**

620

621 **Disclosure Summary**

622 The authors have nothing to disclose.

623

624 **Author Contributions**

625 E.S.J., C.F., B.G., J.M. and G.B.G.G. performed founder generation and transgene experiments. E.S.J., G.W.

626 and P.S. conducted IHC for CTB, PHAL and transgene experiments. E.S.I., E.S.J. and J.A.P.C. analyzed

627 confocal results. E.S.J. and N.Y.R. conducted and analyzed ISH experiments. E.S.J., G.W. and R.M.L.

628 conceived the project and designed experiments. E.S.J., J.L.C. and R.M.L. wrote and edited the manuscript.

629 R.M.L., J.L.C., E.S.J and M.L.O. acquired the funding.

630
631 **Data Availability**
632 All raw data are available on demand.

633
634 **Ethics approval**
635 Protocols followed the NIH guide for the care and use of laboratory animals (8th ed.), and the Official Mexican

636 Norm for production, care and use of laboratory animals NOM-062-ZOO-1999. All experimental protocols

637 were reviewed and approved by the Institutional Animal Care and Use Committee at Tufts Medical Center and

638 Tufts University School of Medicine and the institutional bioethics committees at Instituto de Biotecnología-

639 UNAM and Instituto Nacional de Psiquiatría Ramón de la Fuente Muñiz.

640

641 **Figure legends**

642 **Fig. 1 Localization of CTB injection sites in representative rat brains used for the retrograde tracing**

643 **experiment** A) CTB core localize to E4 in the dorsal TMN (DTMN; bregma approx. -3.72 mm). B-D) CTB

644 cores localize to E1-E2 in the ventral TMN (VTMN; bregma approx. -3.84 mm to -4.20 mm). E) Phase contrast

645 micrography (5x magnification) shows the position of E4-E5 in the dorsal TMN and of E2 in the ventral TMN.

646 MRe= mammillary recess; 3V= 3rd ventricle Scale bar for A-D= 300 μm.

647

648 **Fig. 2 Identification of retrogradely labeled CTB-TRH neurons in the rat tuberal lateral hypothalamus**

649 **(TuLH)** Confocal images from double labeled immunofluorescent cells demonstrate the presence of CTB (red;

650 empty arrows in B, E, H), retrogradely transported from the ventral TMN, accumulating in TuLH pro-TRH

651 neurons (green; empty arrows in A, D, G). White arrows in C, F, I denote double labeled cells. Scale bar shown

652 in I denotes magnification in all micrographs.

653

654 **Fig. 3 Identification of anterogradely labeled (PHAL injection in the tuberal lateral hypothalamus)**

655 **PHAL+TRH-IR fibers in the rat TMN** Upper panels indicate immunolocalization of PHAL (yellow) and

656 TRH (red) in the TuLH at -2.52 mm from the bregma. Two different focal planes for one sample (A, B) were

657 acquired and the Z projection from the original stacks composed of 26 (A) or 32 (B) optical slices, each from

658 two channels: 488 (TRH+) and 561 (PHAL+). The resulting projections of each set were merged and

659 represented as a composite image for planes A and B in C. Arrows and inset point to double labelled cells

660 highlighting in green those which are missing in A or B.

661 Lower panels demonstrate the presence of pro-TRH in PHAL-containing axon terminals or en-passant boutons

662 from TuLH into dorsal (E4, E5) or ventral (E2) TMN. Each channel of the original stack was processed to

663 eliminate its background using an Otsu thresholding algorithm. Then, given a focal plane, each single voxel of

664 the 561 label (PHAL) channel was analyzed to determine if a counterpart existed in the TRH thresholded

665 channel such that the referred voxel could be identified as labeled by two marks. The resultant subset was

666 identified as the set of overlapped voxels and using a yellow lookup table. Once the overlapped voxels were

667 identified, the Z-stack was projected using the standard deviation criteria from the Z projection algorithm of

668 Fiji. The resultant image is overleaped with the Z-projection of the original set of 561 (PHAL) pixels labeled

669 in yellow. Scale bar is shown on each micrograph.

670

671 **Fig. 4 Distribution of *Trh* mRNA in the rat tuberal lateral hypothalamus and *Trh* and *Hdc* mRNA in the**

672 **rat TMN** A) *Trh* distribution in the tuberal lateral hypothalamus (green cells, bregma -2.56 mm) and B-C) in

673 all subdivisions of the TMN (green cells, bregma -3.84 mm). D) Panoramic view of *Hdc* in all subdivisions of

674 TMN (green cells, bregma -3.84 mm). Similar to *Trh* mRNA, *Hdc* mRNA from E1 or E2 accumulates close to

675 the ventral border of the brain while *Hdc+* or *Trh+* cells from E4 and E5 extend horizontally from the

676 mammillary recess to the E2 subdivision. TuLH= tuberal lateral hypothalamus, TMN= tuberomammillary

677 nucleus, MRe3V= mammillary recess of the 3rd ventricle. Scale bar for A= 200 μm; B- C = 50 μm; scale bar

678 for D= 200 μm.

679

680 **Fig. 5 Colocalization of *Hdc* and *Trh* mRNA in the mouse TMN. Double labelled *Hdc+* and *Trh+* mRNA**

681 **cells are observed in all subdivisions of TMN** A) *Hdc+* mRNA (pink) and *Trh+* mRNA (blue), are co-

682 expressed in E1-E2 TMN subdivisions, accumulating close to the ventral border of the brain. B) Double labelled

683 *Hdc+/Trh+* cells in E4-E5 subdivisions extend horizontally from the mammillary recess toward the E2

684 *Hdc+/Trh+* population. White arrows in denote double labeled cells. MRe3V= mammillary recess of the 3rd

685 ventricle. Scale bar = 50 μm.

686

687 **Fig. 6 Identification of anterogradely labeled PHAL+ fibers on *Hdc*+ mRNA or HDC protein cell bodies**

688 **in the mice TMN** A) Double labeling immunolocalization for anti-PHAL (pink) and anti-fluorescein- *Hdc*+

689 (green) mRNA, demonstrates the presence of PHAL anterogradely transported from the TuLH to the TMN.

690 White arrows denote double labeled cells; the yellow arrow denotes an *Hdc*+ cell. B) Immunofluorescence for

691 anti-PHAL (red) anterogradely transported from the TuLH, impinging on a histamine neuron (green) from the

692 TMN. The white arrow denotes a double labeled cell. Nuclei are contrasted with DAPI (blue). Scale bar= 20

693 μm.

694

695 **Fig. 7 Distribution of *Hdc* mRNA in the rat TMN and its relationship with TRH receptors** *Trhr* is

696 expressed in many *Hdc* + (green signal) cells from the TMN (red signal on A), while *Trhr2* expression is low

697 and colocalizes scarcely with *Hdc*+ in the TMN (red signal on B). A´-B´ panels show cells that colocalize *Hdc*

698 and *Trhr*, or *Hdc* and *Trhr2*, mRNAs; images are Z-stacks obtained from each fluorochrome in serial optical

699 cuts of 1 μm. White arrows denote double labeled cells. MRe3V= mammillary recess of the 3rd ventricle. Scale

700 bar for A, B= 50 μm, scale bar for A´, B´=5 μm.

701

702 **Fig. 8 Distribution and activity of *Cre* recombinase in the hypothalamus (TuLH) of TRH-Cre mice** A)

703 The presence of Cre was mapped in the progeny of TRH-Cre x reporter mice carrying the GFP gene flanked by

704 Lox-P sequences. GFP+ cells were detected by immunochemistry in brain slices containing the dorsomedial

705 nuclei and the lateral hypothalamus including perifornical cells and the TuLH, where *Trh* mRNA is expressed.

706 B) Fluorescent *in situ* hybridization for *Trh* (green signal) or *Cre* recombinase (red signal) mRNA in 10 μm

707 coronal sections from the TuLH of TRH-Cre male mice. Sections were hybridized with *Trh* digoxigenin-UTP

708 and *Cre* fluorescein- UTP cRNA probes and developed with anti-dig-POD/TSA biotin and Alexa 488 secondary

709 antibody for *Trh* and anti-fluorescein/Cy3 secondary antibodies for *Cre*. White arrows point to *Trh*+ or *Cre*+

710 cells obtained from Z-stacks for each fluorochrome at 488 (*Trh*) or 561 (*Cre*) emission channels. C) Cre-

711 dependent reporter protein mCherry expression is observed 6 weeks after inoculation in the TuLH of a floxed

712 adeno-associated virus (AAV) vector (white signal) but not in the neighboring TRH+ cells from the dorsomedial

713 nuclei (DMN; green signal). D) Immunohistochemistry for mCherry+ in TRH-Cre mice inoculated with a

714 floxed-AAV-mCherry in the TuLH, allows to easily differentiate cell bodies as well as extensions of mCherry+

715   cells in the rostral and caudal hypothalamus; arrows denote Cre-mCherry positive fibers in the lateral septum.

716   Scale bar on A= 400 µm; B= 50 µm; confocal stacks= 5 µm. DMNd, dorsomedial hypothalamic nucleus dorsal;

717   DMNv, dorsomedial hypothalamic nucleus ventral; ic, internal capsule; ME, median eminence; MTu, medial

718   tuberal nucleus; PeFLH, perifornical part of lateral hypothalamus; PLH, peduncular part of lateral

719   hypothalamus; sox, supraoptic decussation; TuLH, tuberal region of lateral hypothalamus; LV, lateral ventricle;

720   dTMN, dorsal tuberomammillary nucleus; vTMN, ventral tuberomammillary nucleus; III, 3rd ventricle.

721

722   **Fig. 9 Identification of TMN TRH-IR fibers anterogradely labeled through the intra TuLH injection of**

723   **a floxed-AAV-mCherry in *Trh-Cre* mice** mCherry was observed, 6 weeks after AAV inoculation, in the

724   tuberal lateral hypothalamus (TuLH) and TMN subregions as E1, E2. Cell bodies as well as extensions of

725   mCherry+ cells are easily differentiated (upper panels). Lower panels demonstrate the presence of pro-TRH in

726   mCherry-containing axon terminals or en-passant boutons from TuLH into the ventral (E1, E2) TMN. A Z-

727   stack formed by 26 planes (separated by one micron) was acquired using a CSU-W1 Yokogawa SDC on an

728   inverted Zeiss microscope Observer Z1 with a Z-stage ASI Piezo MS- 2000 Controller. Each single plane is

729   composed by two fluorescence channels 488 nm (TRH) and 561 nm (mCherry). The analysis was based on a

730   graphical representation of Manders criteria named Manders co-localization map (Manders, 1993). This process

731   starts with a background elimination process performed by mean of an Otsu thresholding algorithm. Then, given

732   a focal plane, each single voxel of the 561 label (mCherry) channel was analyzed to determine if a counterpart

733   existed in the TRH thresholded channel such that the referred voxel could be identified as labeled by two marks.

734   The resultant subset was identified as the set of overlapped voxels and use of magenta lookup table. Once the

735   overlapped voxels were identified, the Z-Stack was projected using the Standard deviation criteria from the Z

736   projection algorithm of Fiji. The resultant image was overleaped with the Z-projection of the original set of 561

737   (mCherry) pixels labeled in red. Scale bar is shown on each micrograph.

738

739

740   **Supplemental figure legends**

741   **Fig. S1 Distribution of a Cre reporter in the CNS of the TRH-Cre mice. The presence of Cre was mapped**

742   **in the progeny of TRH-Cre x reporter mice carrying the GFP gene flanked by Lox-P sequences** GFP was

743 detected by immunohistochemistry. In the CNS, GFP+ cells are distributed where *Trh* mRNA is expressed.

744 Scale bar= 400 μm. DMNd, dorsomedial hypothalamic nucleus dorsal; fx, fornix; ic, internal capsule; LV,

745 lateral ventricle; ME, medium eminence; MPOM, medial preoptic nucleus; MRe, mammillary recess of the 3rd

746 ventricle; mt, mammillothalamic tract; MTu, medial tuberal nucleus; OB, olfactory bulb; opt, optic tract; PaAP,

747 paraventricular hypothalamic anterior parvicellular; PaMP, paraventricular hypothalamic medial parvicellular;

748 pe, periventricular hypothalamic nucleus; PeFLH, perifornical part of lateral hypothalamus; pfx, perifornical;

749 PLH, peduncular part of lateral hypothalamus; POA, preoptic area; sox, supraoptic decussation; TuLH, tuberal

750 region of lateral hypothalamus; TMN, tuberomammillary nucleus, dorsal (dTMN) and ventral (vTMN); VLPO,

751 ventrolateral preoptic area; VMN, ventromedial hypothalamic nucleus; III, 3rd ventricle.

752

753 **Fig. S2 Distribution and activity of *Cre* recombinase in the PVN, thalamus and pituitary of TRH-Cre**

754 **mice** A) Fluorescent in situ hybridization for *Trh* or *Cre* recombinase mRNAs in coronal sections containing

755 the thalamus and the hypothalamic paraventricular nucleus (PVN) of C57/BL6JN male mice (left) and TRH-

756 Cre male mice (right); sections were hybridized with digoxigenin-UTP cRNA probes and developed with

757 biotin-tyramide (BT)-AMCA Avidin D. B) Signal distribution for *Trh* and *Cre* mRNA shown in A) are

758 compared to that reported for *Trh* mRNA on the Allen Brain Atlas; arrow in the inset points to the mediodorsal

759 thalamic nucleus (MD). C) Endogenous *Trh* mRNA was detected with a ^{35}S UTP-labeled cRNA probe in

760 C57/BL6JN male mice (left); immunofluorescence for ß-gal was performed in the offspring of TRH-Cre x

761 ROSA 26 mice (right). Distribution pattern for *Trh* ^{35}S mRNA in the PVN, was similar to that for *Trh* developed

762 with BT-AMCA in A) or alkaline phosphatase in B) and *Cre* mRNA in A) or immunofluorescence for ß-gal in

763 C). Lower panels in C show double-labeling immunofluorescence for ß-gal and TSH in the anterior pituitary

764 demonstrating that *Cre* expression is excluded from TSH cells, as does that of *Trh*. Double-labeling

765 immunofluorescence for ß-gal and GH in the anterior pituitary demonstrates that Cre expression occurs in some

766 growth hormone (GH) cells, as expected; double-labeled cells are denoted by the yellow signal. D3V= dorsal

767 3rd ventricle; AD= anterodorsal thalamic nucleus; sm= stria medullaris of the thalamus; MD= mediodorsal

768 thalamic nucleus, Rt= reticular thalamic nucleus; SFO= subfornical organ; PVN= hypothalamic paraventricular

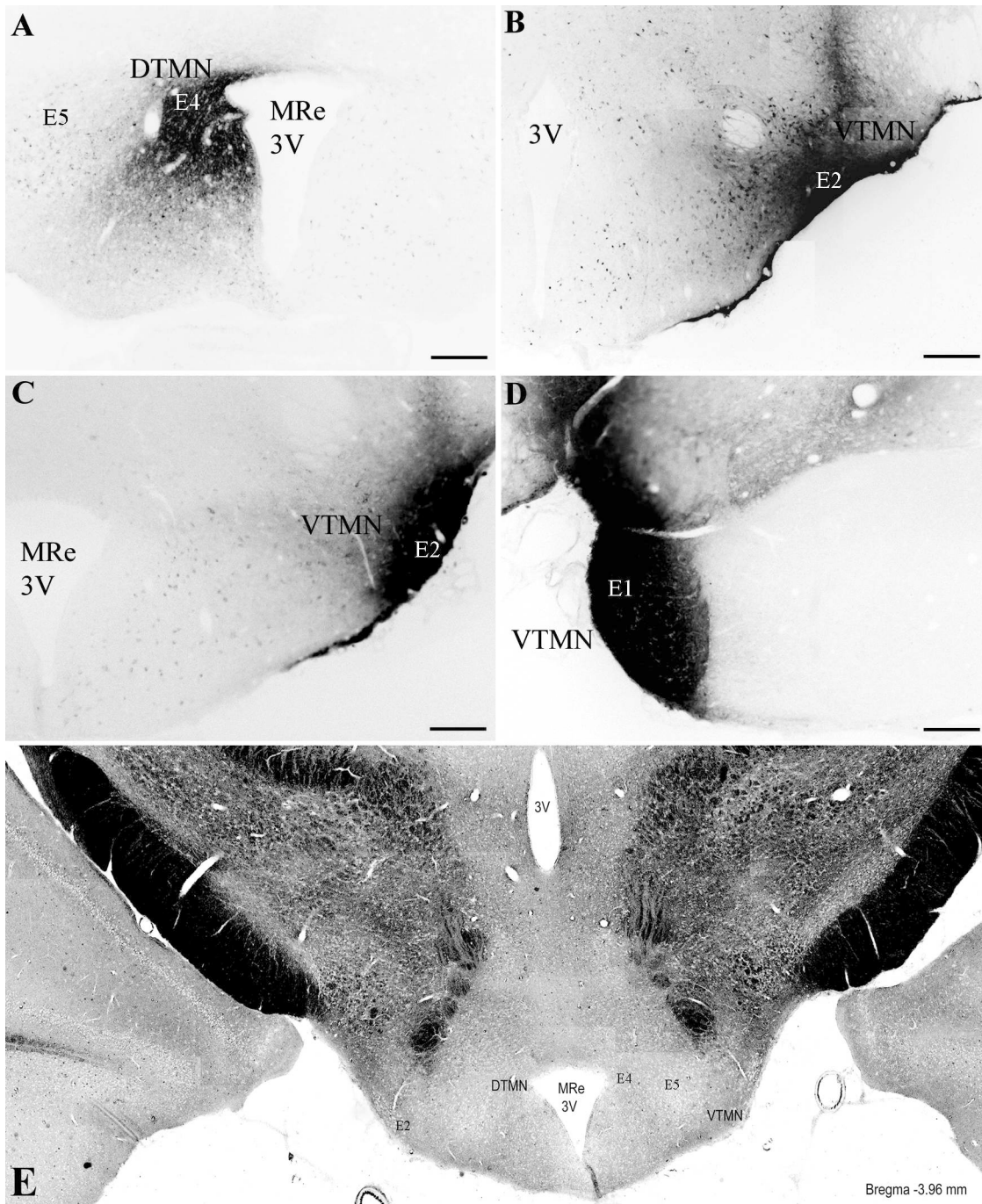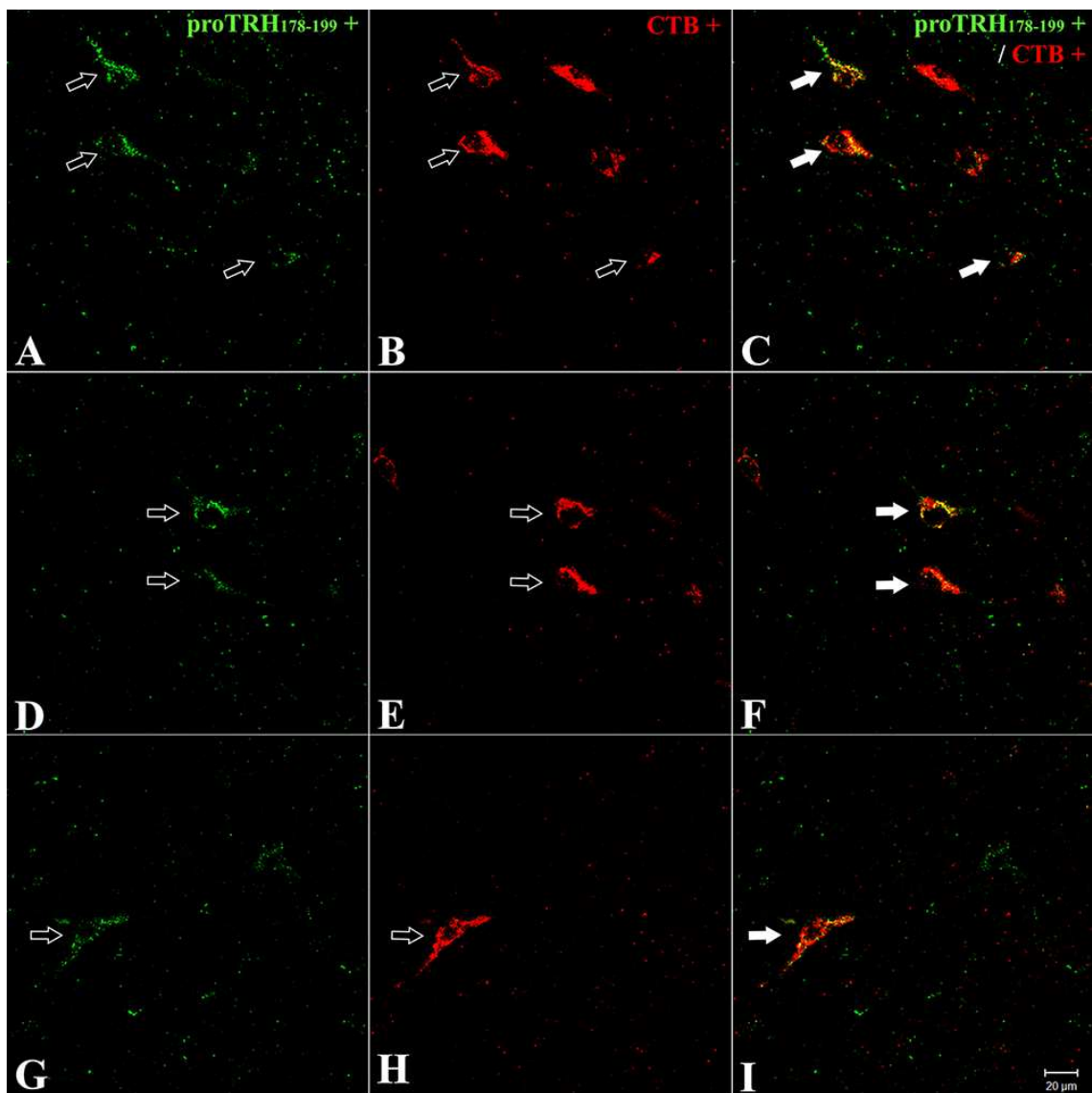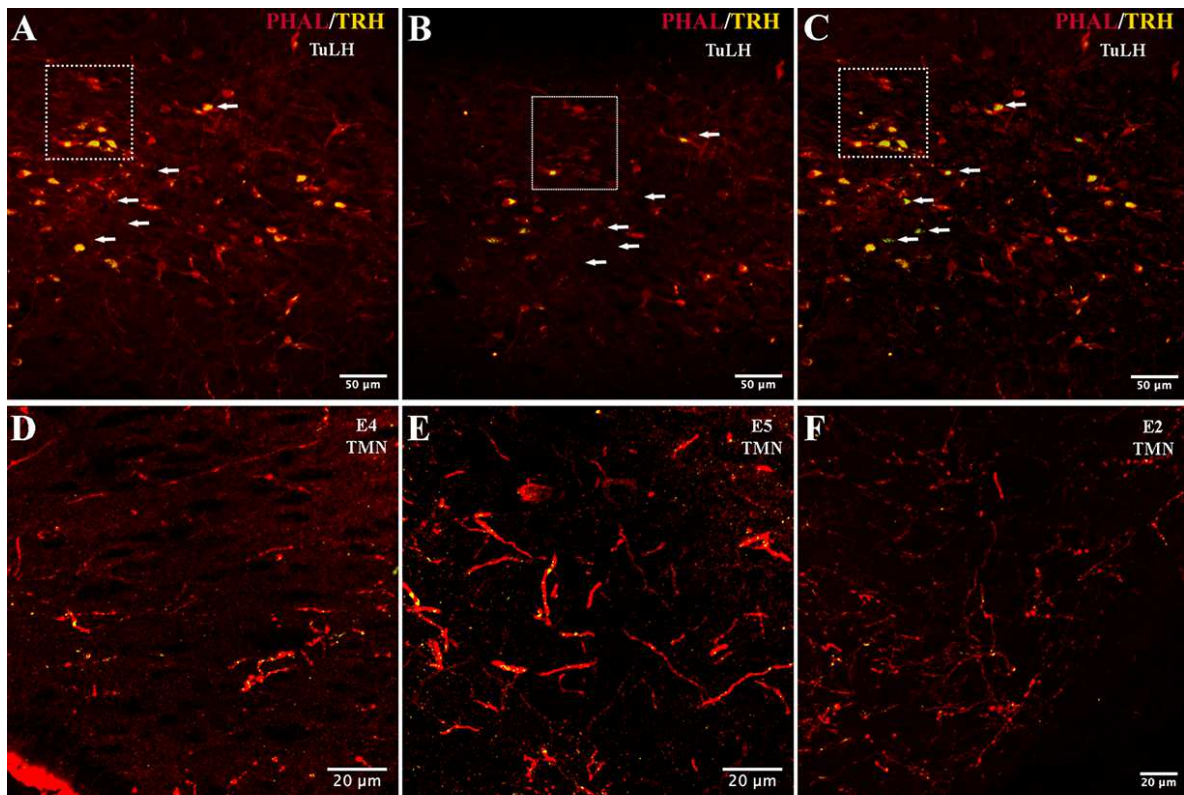769 nucleus; III= 3rd ventricle; AP= anterior pituitary.

770

Fig. 1

proTRH178-199 +

CTB +

proTRH178-199 + / CTB +

A

B

C

D

E

F

G

H

I

20 µm

773 **Fig. 2**

28

Fig. 3

774

Fig. 4

775

Fig. 5

A: *Hdc*+ / PHAL+

B: HDC+/PHAL+/DAPI+

777   **Fig. 6**

778　**Fig. 7**

779 **Fig. 8**

TRH/Cherry

TuLH

TuLH

E2

E1

100 μm

100 μm

20 μm

20 μm

Fig. 9

781 **Fig. S1**

782 **Fig. S2**